Numerical Simulations of Canted Nozzle and Scarfed Nozzle Flow Fields

Afroz Javed & Debasis Chakraborty

Journal of The Institution of Engineers (India): Series C
Mechanical, Production, Aerospace and Marine Engineering

ISSN 2250-0545
Volume 98
Number 5

J. Inst. Eng. India Ser. C (2017)
98:625-633
DOI 10.1007/s40032-016-0305-2

Springer

J. Inst. Eng. India Ser. C (October 2017) 98(5):625–633
DOI 10.1007/s40032-016-0305-2

CASE STUDY

Numerical Simulations of Canted Nozzle and Scarfed Nozzle Flow Fields

Afroz Javed[1] · **Debasis Chakraborty**[1]

Received: 26 November 2014 / Accepted: 20 May 2016 / Published online: 18 June 2016

Abstract Computational fluid dynamics (CFD) techniques are used for the analysis of issues concerning non-conventional (canted and scarfed) nozzle flow fields. Numerical simulations are carried out for the quality of flow in terms of axisymmetric nature at the inlet of canted nozzles of a rocket motor. Two different nozzle geometries are examined. The analysis of these simulation results shows that the flow field at the entry of the nozzles is non axisymmetric at the start of the motor. With time this asymmetry diminishes, also the flow becomes symmetric before the nozzle throat, indicating no misalignment of thrust vector with the nozzle axis. The qualitative flow fields at the inlet of the nozzles are used in selecting the geometry with lesser flow asymmetry. Further CFD methodology is used to analyse flow field of a scarfed nozzle for the evaluation of thrust developed and its direction. This work demonstrates the capability of the CFD based methods for the nozzle analysis problems which were earlier solved only approximately by making simplifying assumptions and semi empirical methods.

Keywords Canted nozzle · Inlet flowfield · CFD · Scarfed nozzle

Introduction

Traditionally, the rocket motor and nozzle system are located in the rear of the missile with the axis of the nozzle oriented along the missile centreline. However, the guidance requirements of several existing and proposed tactical missiles necessitate the location of guidance and control equipment (actuators, receivers, wire reels etc.) in the aft region. Therefore, with these demands on the rear of the missile, propulsion system needs to be moved forward. For such applications, the nozzle axis can no longer be on the missile axis; instead, the nozzles are canted at an angle to the missile centreline. Such nozzles are generally called as canted, vectored, or tilted nozzles. Unbalanced side force is generated in canted nozzle and the resultant thrust vector does not lie along the missile axis or nozzle axis. When two or more canted nozzles are located symmetrically around the missile axis, resultant thrust vector coincide with the missile axis. However, even in that case, missile axial thrust is reduced below the nozzle axial thrust because of nonalignment of missile and nozzle axes. The typical arrangement of two canted nozzles placed symmetrically around the missile axis is shown in Fig. 1a. Sometimes, due to aerodynamic considerations the protruding nozzle part needs to be flushed with the missile body. Such nozzles are called scarfed nozzles. A schematic view of twin scarfed nozzles configuration is shown in Fig. 1b.

In yester years, the performance prediction [1–3] of such nozzles used to be based on two-dimensional axisymmetric flow field model using the method of characteristics solution technique. Recent advances in parallel computers, robust numerical algorithms and maturity of CFD codes are enabling the designer to use them as design tools to study detailed three dimensional flow fields without much turnaround time. The standard practice for nozzle performance analysis is to assume a uniform axisymmetric flow field at the inlet, generally defined by total pressure and total temperature. This assumption is quite satisfactory owing to the low velocities and sufficient space before nozzle entry

✉ Afroz Javed
afrozjaved@gmail.com

[1] Defence Research and Development Laboratory, Hyderabad 500058, Telangana, India

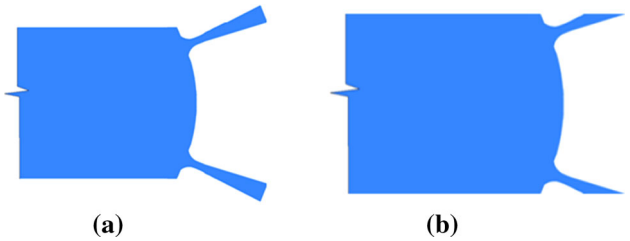

Fig. 1 Schematic arrangement of **a** twin canted nozzle **b** twin canted and scarfed nozzle

in most solid rocket motor designs. In solid rocket motors with multiple nozzles and end burning grains, the entry flow field neither remains uniform nor axisymmetric. The asymmetry of the flow at the nozzle entry is further enhanced when the nozzles are canted.

Very few studies are reported in open literature for the non axisymmetric inlet condition at the canted nozzle inlets. One such study has been carried out by Zhang et al. [4], where the non-uniform flow field at the inlets of straight and canted nozzles are analysed using computational techniques. In this study it is reported that a nozzle which is straight, when gimballed does not show a significant increase in throat erosion characteristics for a double base propellant system.

In the present work CFD techniques are used to study the axisymmetry of inlet flow field of canted nozzles of an end burning rocket with double base propellant. In this rocket, the products of combustion are exhausted from two conical nozzles at the end of the motor as shown in Fig. 1. Two sets of nozzle geometries as shown in Fig. 2 are considered, and a flow field analysis is carried out for four different burn back geometries in each case to assess the non-axisymmetric nature of the flow field. The CFD study is carried out to select the geometry with better inlet flow field in terms of symmetry, out of the two available designs.

In case of canted nozzles, the evaluation of thrust and its direction is straightforward. However for scarfed nozzles the thrust and its direction can be evaluated using semi-empirical relationships or methods of characteristics with some simplifying assumptions. In the present work CFD techniques are utilised to evaluate the thrust and its direction for a scarfed nozzle configuration.

Geometries and Grids for Canted Nozzle

The rocket motor considered, is fitted with two convergent–divergent nozzles canted at an angle from the motor axis. The nozzles are designed with high temperature resistant materials in the convergent and throat part to stand high temperature flow from the motor.

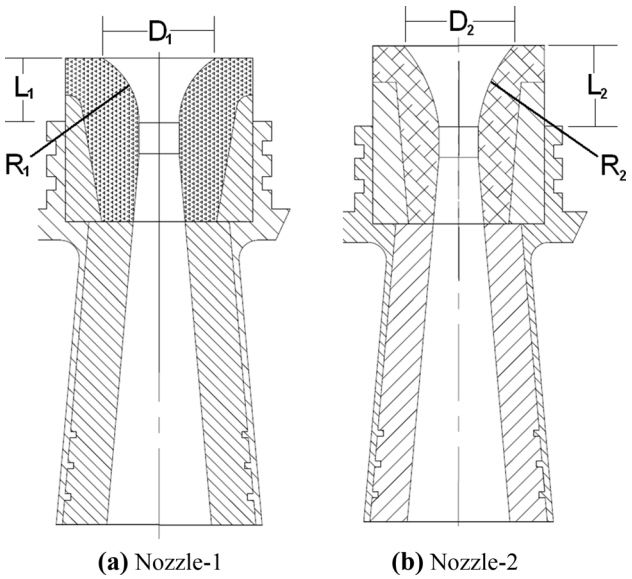

Fig. 2 Nozzle geometries for the two nozzles. **a** Nozzle-1. **b** Nozzle-2

When the combustion of the end burning grain starts the burning surface is very near to the nozzle entry, as the combustion proceeds the burning surface recedes and the distance between the burning surface and nozzle entry increases. The rate of grain burn back is of the order of few millimetres per second, while the velocity of the combustion gases near the inlet is of the order of 10–100 m/s. With this difference in the two time scales, the phenomena of grain recession and flow field development can be decoupled in time and steady state simulations could be performed for the flow field with the assumption of a non moving boundary at the grain surface. In order to analyse the flow fields at different burning times, four burning instants are chosen. At these burn instants the grain surface locations from the starting of combustion are 0, 32, 85 and 160 mm. The location of the burning surface is evaluated based on the burn rate of the propellant. The computational domains at these conditions are shown in Fig. 3. It can be noticed that only half the geometry consisting of one nozzle is considered taking advantage of the symmetry.

The computational grids are made using ICEM CFD software [5]. Hexahedral grids with clustering near the flow gradients are made. Table 1 shows the number of grids considered for different simulations.

Geometry and Grids for Scarfed Nozzle

The schematic of the nozzle geometry with boundary locations and co-ordinate directions is shown in Fig. 4. In the present case the scarfed nozzle inlet is axi-

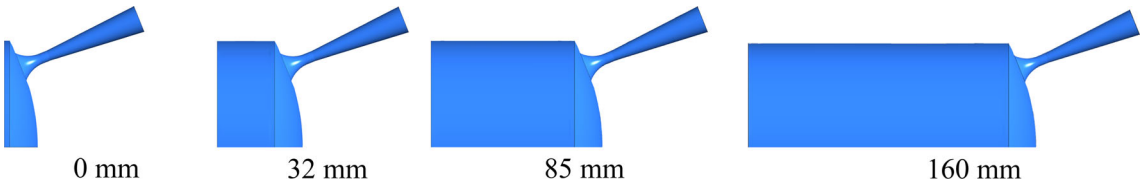

Fig. 3 Domains considered for the flow simulations at different time instants

Table 1 Number of grids considered for simulations

Geometry	0 mm	32 mm	85 mm	160 mm
Grid size (millions)	0.68	0.95	1.18	1.63

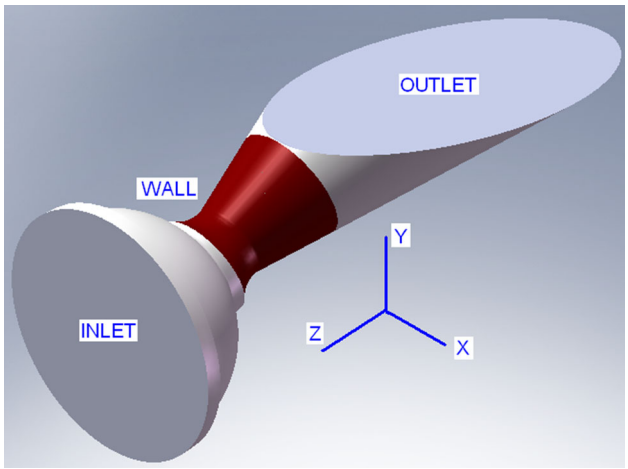

Fig. 4 Schematic of nozzle geometry with boundary locations and co-ordinate directions

symmetrically located on the rocket motor; hence the inlet flow field is expected to be symmetric in nature. With symmetric inlet flow field, the flow simulation in the rocket motor grain portion is not required and only nozzle is considered. ICEM CFD software [5] is used to generate structured grids for the flow domain. A total of around 0.8 million hexahedral grids are used for the simulation of the nozzle flow field. The grids are clustered near the walls to capture the boundary layer and resulting flow gradients.

Solution Methodology

The flow features in the solution domain are evaluated by solving three dimensional Reynolds Averaged Navier–Stokes (RANS) equations using CFX 11 software [6], which is capable of solving diverse and complex multidimensional fluid flow problems. The code uses finite volume method with finite element based discretization of geometry with fully implicit numerical schemes. Turbulence is modelled through k–ε turbulence model suggested by Launder and Spalding [7]. The convective terms in mass, momentum, and energy equations are discretized through 2nd order scheme, while first order scheme is used for the discretization of turbulence transport equations. Log-normalized maximum residue of −04 is considered as the convergence criteria. The governing equations and the discretization schemes are discussed in detail by Javed et al. [8] for non reacting flow simulations of blast tubes. To find out the accuracy and the range of applications, the software has been validated for various internal flow fields in air intakes [9], dual pulse rocket motor [10], rectangular duct behind backward facing step [11, 12] etc. and good quantitative agreement is obtained between experimental and computational results.

The reactions occurring in the solid propellant resulting in the generation of the gaseous products are not used in the solution of the flow field; instead, it is assumed that all the products of combustion are available in equilibrium state very near to the burning surface in gaseous form. Considering the high rates of reactions in solid propellant combustion, this assumption is satisfactory. The thermo chemical and transport properties for the exhaust gases (products of combustion) are evaluated using NASA CEA 600 programme [13, 14], as shown in Table 2.

Boundary Conditions for Canted Nozzles

The boundary conditions are defined as the grain burning surface to be a subsonic inlet with a mass flow rate specified. No slip adiabatic wall condition is specified at the wall and an atmospheric pressure boundary condition is given at the outlet. The typical locations of these boundaries are shown in Fig. 5.

Table 2 Thermo chemical and transport properties

Property	Value for canted nozzles	Value for scarfed nozzle
Total temperature	3083 K	3400
Molecular weight	26.55	28
Ratio of specific heats	1.24	1.19
Thermal conductivity	0.21 W/mK	0.42412 W/mK
Dynamic viscosity	6.45×10^{-6} Pa s	9.34×10^{-5} Pa s

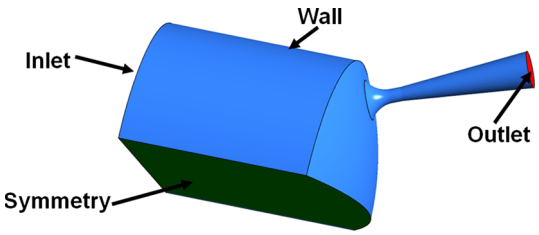

Fig. 5 Flow domain for simulations with the boundary conditions

Boundary Conditions for Scarfed Nozzle

The boundary locations are shown in Fig. 4 for this case. A total pressure boundary condition is given at the nozzle inlet with total temperature. The outlet boundary condition is kept as supersonic. The walls are adiabatic with no slip condition.

Numerical simulations are carried out with a global time step of 1×10^{-4} s. A convergence level of 1×10^{-4} on maximum residuals is achieved for all the simulations. These converged results are used for post processing and data extraction.

Results and Discussions

Canted Nozzles

The two nozzles considered, differ in their inlet diameters and radii of curvature in the convergent portions. The velocity distributions for Nozzle-1 and Nozzle-2 at initial burn surface location (0 mm) are shown in Fig. 6. It can be observed that the flow accelerates from very low velocities near the inlet to high subsonic velocities in the convergent portion and reaches sonic velocity (1034 m/s) at the throat and further acceleration occurs in the divergent portion till the exit of the nozzle to a velocity of 2453 m/s at the nozzle exit. A further examination shows nearly the same velocity distribution in both the nozzle geometries. However, the range of velocities existing in the nozzles is very large varying from zero near walls to around 2453 m/s at the exit of the nozzles which makes it difficult to observe the differences in the region near inlets and convergent portions. In order to observe the flow fields near the inlets, areas of interest near the inlets are zoomed and shown in Fig. 7 at different locations of burn surfaces. The scale of velocity is also zoomed to show velocities only from zero to 100 m/s. This zooming of velocity scale makes all the velocities equal to or greater than 100 m/s to be in same colour (red). An examination of Fig. 7 shows that the velocity distribution near the inlet at 0 mm location of burn surface is not symmetric. It can also be observed that the velocity in the region of inlet away from centre of motor chamber is of the order of 100 m/s, while that in the regions near to the centre of motor chamber is 50 m/s. Slight difference in the flow fields for both the nozzle geometries is observed at the initial grain position. As the grain recedes no noticeable difference can be made out from the plots shown in Fig. 7. For closer examination of the flow fields at the inlets of the nozzles axial velocity distributions are plotted at the nozzles inlet planes for different grain positions in Fig. 8. From this figure it can be observed that at initial grain position (0 mm) the flow is qualitatively more axisymmetric for Nozzle-2 geometry. As the grain recedes the flow field becomes more axisymmetric for both the geometries, however, the

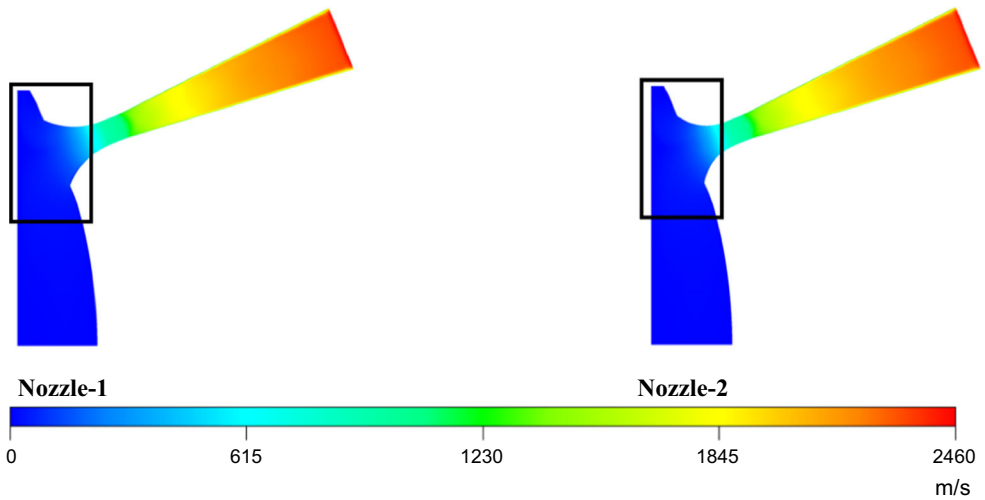

Fig. 6 Distribution of velocity in the nozzle for the two geometries

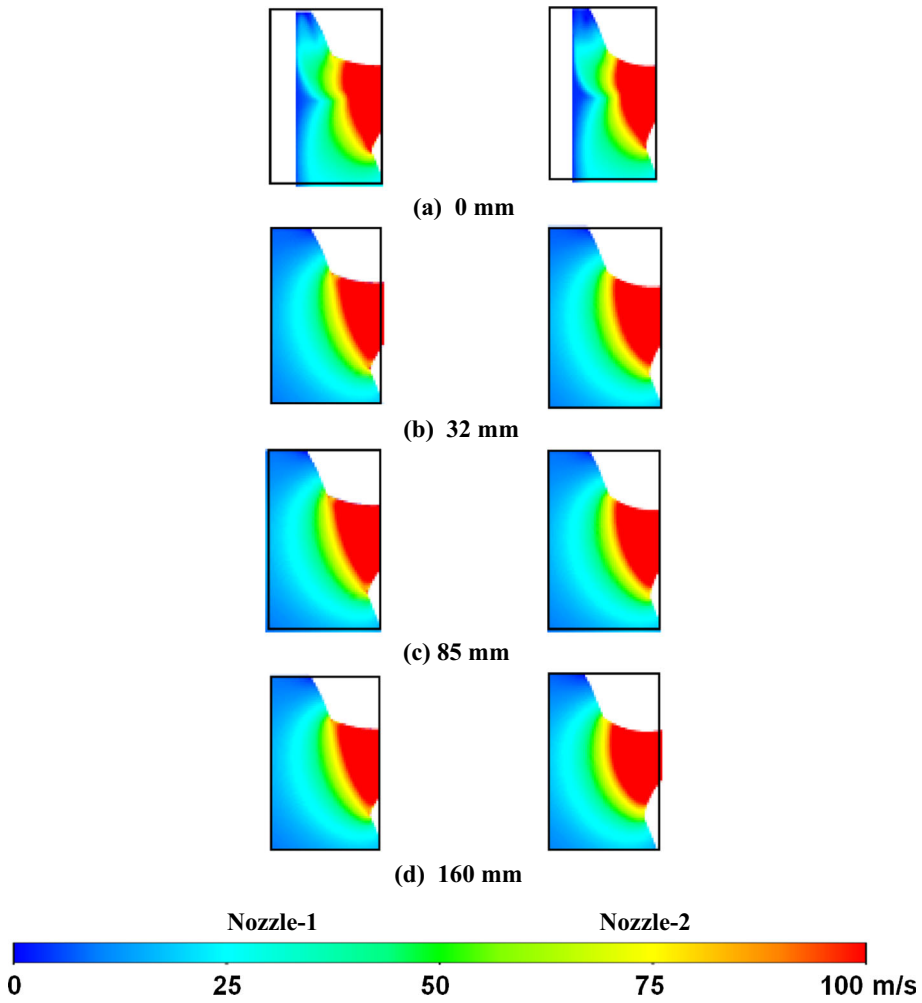

Fig. 7 Distribution of velocity for the two geometries near nozzle entrance at different grain burn back locations. **a** 0 mm, **b** 32 mm, **c** 85 mm, and **d** 132 mm. (Distance of burn back geometry is measured from the initial location of grain surface)

velocities near the walls are higher for Nozzle-1 case than those observed for Nozzle-2.

In order to further analyse the asymmetry of the flow at the inlet of the nozzles, wall pressure difference values in the azimuthal direction for Nozzle-1 and Nozzle-2 are shown in Fig. 9 for different grain positions. The pressures differences are evaluated by subtracting the wall pressure value on a point farthest from the centre line of the motor (designated as zero degree on the azimuthal line) from the local values. It can be seen that the differences in the wall pressure values in azimuthal direction are higher (peak values differ by 33 %) for Nozzle-1 as compared with those for Nozzle-2 at the initial grain position (0 mm). With the regression of the burning surface the pressure differences can be observed to reduce. The variation in wall pressures in the azimuthal direction at nozzle inlets is quantified in terms of standard deviation from its average values. These standard deviations are shown in Fig. 10. The examination of this figure reveals that the standard deviation in the wall pressure from its average value is highest at 0 mm grain position with higher value for Nozzle-1. As the grain position moves away from the nozzle inlet the deviations in the wall pressures from average values get reduced with nearly the same values for Nozzle-1 and Nozzle-2.

From the previous discussions it is observed that the flow field at the nozzles inlets is non axisymmetric initially. This observation raises a concern about the direction of the thrust vector during the initial phase of operation. In order to check the flow asymmetry with axial location, constant Mach number lines are drawn in Fig. 11 for both nozzle geometries at initial grain position. It can be observed that the asymmetry in the Mach number is reduced in the downstream direction. By the time the flow reaches a Mach number of 0.4 in the convergent section of the nozzles, it becomes completely axisymmetric. Achieving axisymmetry by the flow before the nozzle throat ensures the thrust axis to be aligned with nozzle axis even though the flow entering the nozzle is not axisymmetric.

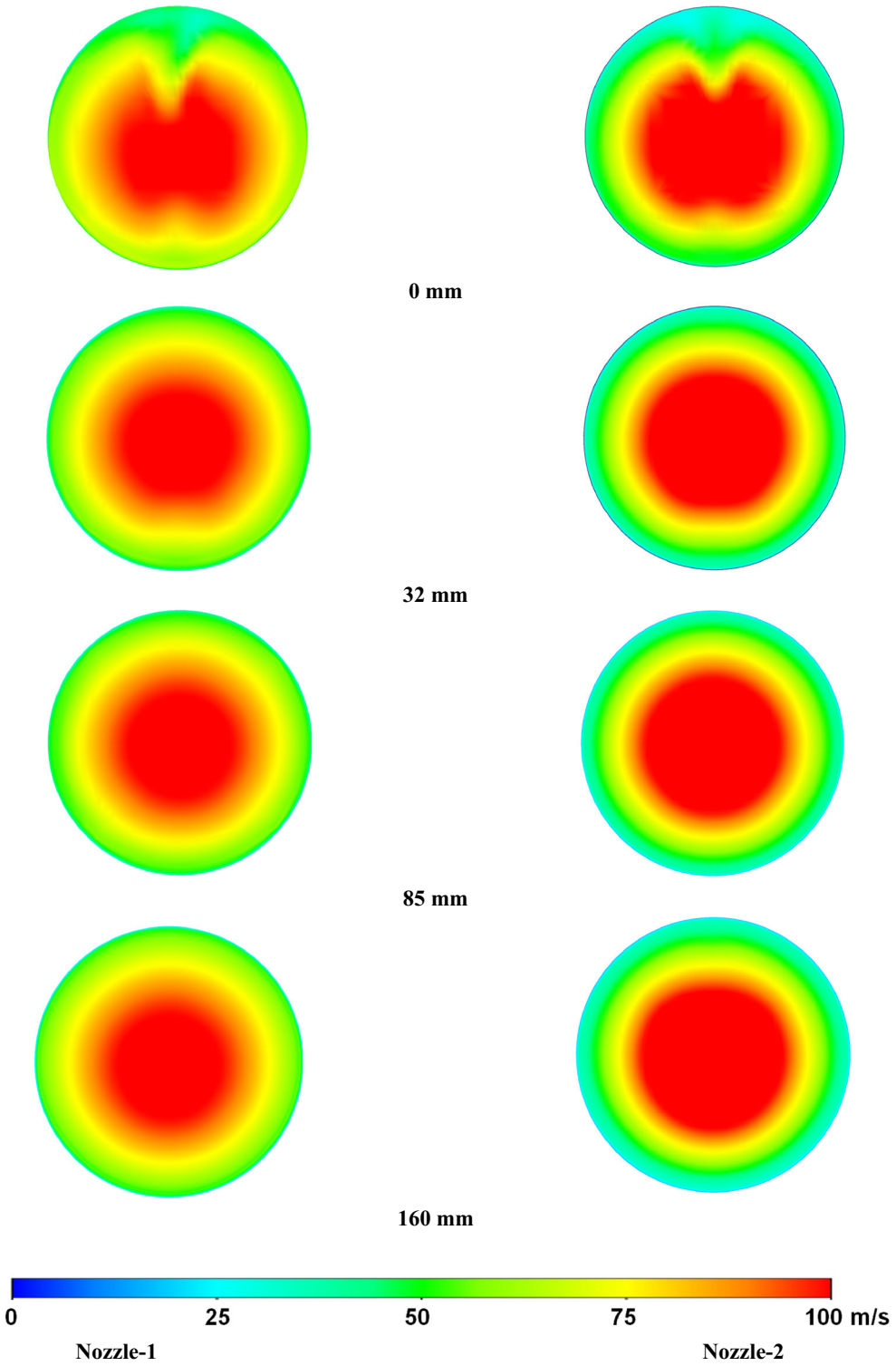

Fig. 8 Distribution of axial velocity in the inlet plane for the two geometries at different grain burn back locations

Scarfed Nozzle

The Mach number variation in the symmetry plane of the nozzle is shown in Fig. 12. It can be observed that a maximum Mach number of 3.38 is reached at the tip of the nozzle; also some weak waves are observed in the nozzle diverging section. The distribution of velocities in axial (z) and perpendicular (y) directions at the outlet plane are

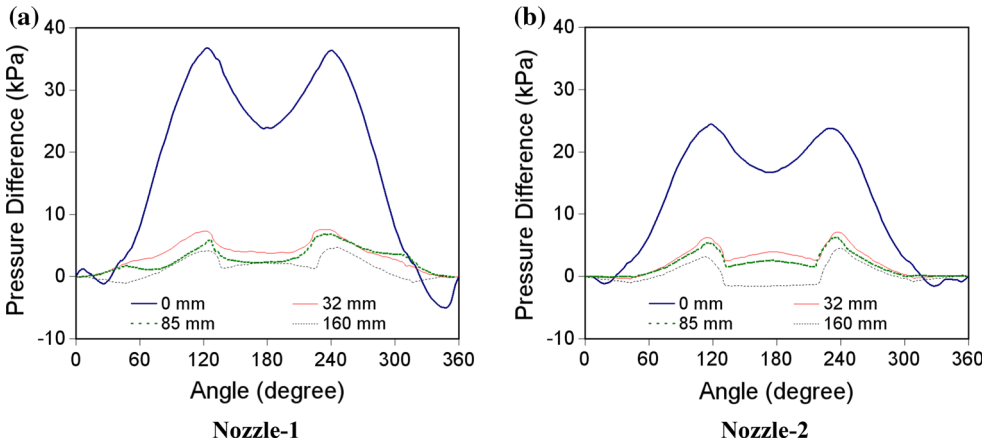

Fig. 9 Wall pressure difference in azimuthal direction on the inlet planes of Nozzle-1 and Nozzle-2 with the grain position

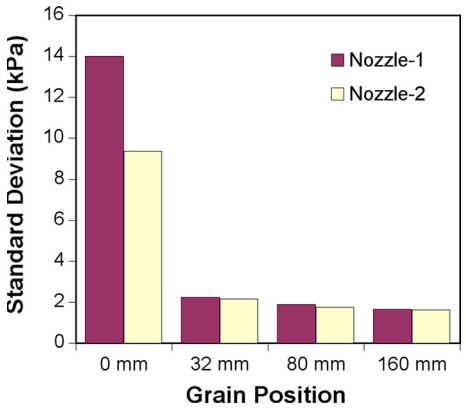

Fig. 10 Standard deviation of pressure in azimuthal direction from its average value at the inlet of nozzles

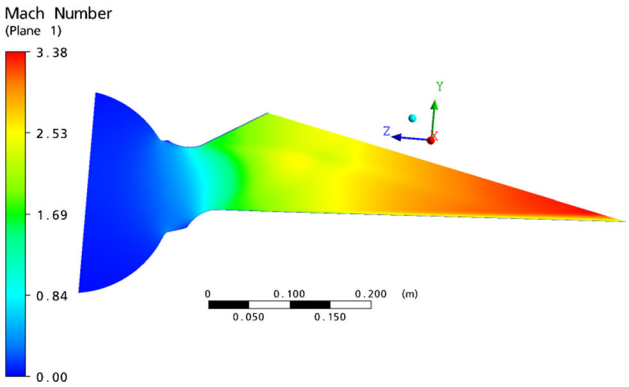

Fig. 12 Mach number distribution in the symmetry plane

shown in Fig. 13a, b respectively. The axial velocity has its maximum value of 2636 m/s at the tip of nozzle while the perpendicular component of the velocity has its maximum value of 1006 m/s at the beginning of the exit plane.

Figure 14 depicts the static pressure distribution at the outlet plane. An examination of this figure shows a maximum value at the beginning of the exit plane while the minimum pressure occurs at the tip of the nozzle. The minimum value of pressure is 1.05 bar which is slightly higher than the atmospheric pressure (1.01 bar). Due to this higher pressure at the exit, the assumption of supersonic flow as the exit boundary condition is justified.

In order to evaluate the thrust from this nozzle the momentum thrusts in the two directions are evaluated using the mass averaged values of the velocities in the two perpendicular directions. The momentum thrusts in y direction

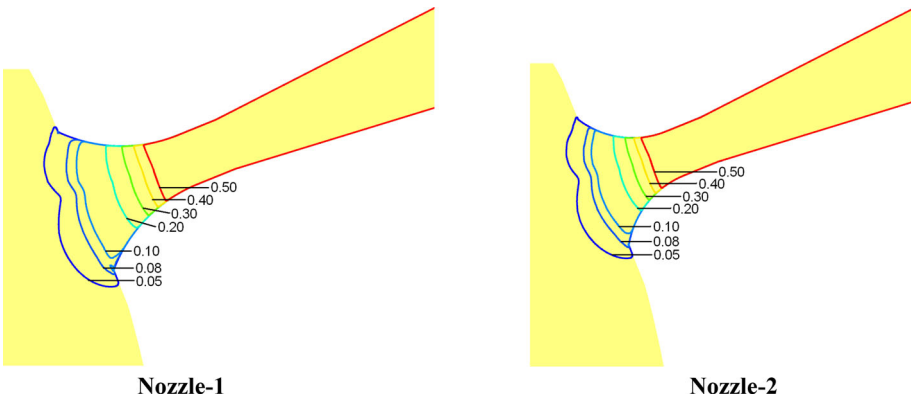

Fig. 11 Constant Mach number lines for initial grain location at axial cross section

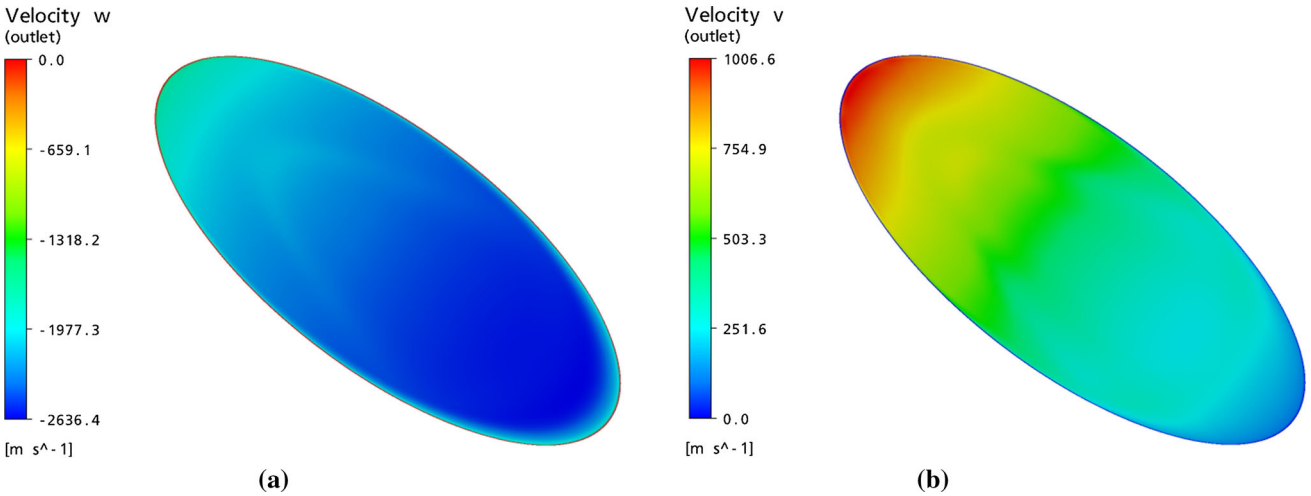

Fig. 13 Velocity distribution in the outlet plane. **a** Axial velocity. **b** Perpendicular velocity

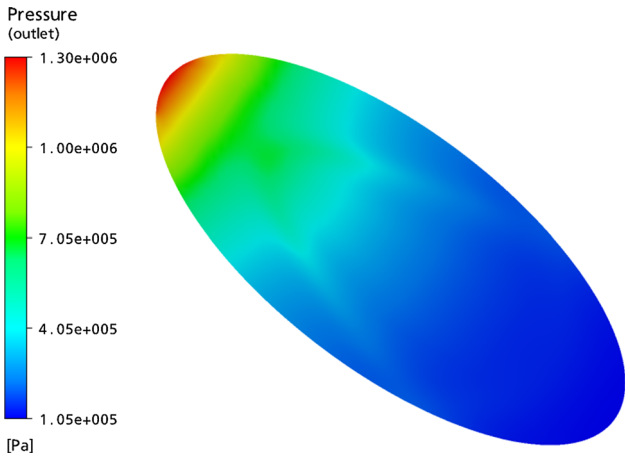

Fig. 14 Pressure distribution in the outlet plane

and z direction are given as $Fm_y = \dot{m}\,v = 26.2\,\text{kN}$ and $Fm_z = \dot{m}\,w = 91.2\,\text{kN}$ respectively. The pressure thrust is evaluated as $Fp = (p - p_a)A_e = 17.97$ kN at sea level atmospheric conditions. The direction of the pressure thrust is perpendicular to the nozzle exit plane. While evaluating these thrust values the values of the different variables are taken as mass flow rate through nozzle $\dot{m} = 41.679\,\text{kg/s}$, mass averaged axial velocity $w = 2187.35$ m/s, mass averaged perpendicular velocity $v = 628.63$ m/s, area averaged exit plane pressure $p = 3.48$ bar, and exit plane area $A_e = 72.46 \times 10^{-3}\,\text{m}^2$. The exit plane of the nozzle makes an angle of 12° from the z axis. The resultant thrust of both momentum and pressure component in y and z directions are given as $F_y = Fm_y + Fp{\cdot}\cos 12^\circ = 43.8$ kN and $F_z = Fm_z + Fp{\cdot}\sin 12^\circ = 94.9$ kN respectively. The magnitude of total thrust comes out to be $F = \sqrt{F_y^2 + F_z^2} = 104.5\,\text{kN}$. The angle made by the thrust vector from the z axis is evaluated as $\theta = \tan^{-1}\left(\frac{F_y}{F_z}\right) = 24.8^\circ$.

This study demonstrates the efficacy of CFD techniques for the performance evaluation of scarfed nozzles without making use of simplifying assumptions.

Conclusions

Numerical simulations are carried out for the quality of flow in terms of axisymmetric nature, at the inlet of canted nozzles of a rocket motor. Two different nozzle geometries are examined and the quasi steady state flow field is numerically evaluated for both the geometries at different grain burn back distances. The analysis of these simulation results shows that the flow field at the entry of the nozzles is non axisymmetric at the start of the motor. This asymmetry arises because of the position of nozzle on the motor as well as the canting. This flow asymmetry at the entry is found to reduce and finally vanish with the passage of time. Comparison of the flow fields for two nozzle geometries shows that the flow symmetry is slightly better for the Nozzle-2 geometry as compared with Nozzle-1. Also it is found that the flow velocities near the nozzle walls are comparatively higher for Nozzle-1 geometry, while for the Nozzle-2 geometry high speed flow is concentrated towards the nozzle axis. With this kind of distribution of axial velocities in terms of axisymmetric nature and its values near the wall, Nozzle-2 configuration appears to be better than Nozzle-1 configuration. Also the axial distributions of Mach numbers in both the geometries indicate that the flow field becomes axisymmetric near/before the nozzle throat and the thrust vector would not have any misalignment with the nozzle axis.

A 3-D RANS simulation has been carried out for the scarfed nozzle also. Thrust from the nozzle is evaluated

using the simulation results. The direction of the thrust is also evaluated using the values of the axial and perpendicular components of the thrust. This study demonstrates the efficacy of CFD techniques for the performance evaluation of scarfed nozzles without making use of simplifying assumptions.

Acknowledgments This paper is a revised version of an article entitled ''Numerical Simulations of Canted Nozzle and Scarfed Nozzle Flow Fields'' presented at the Twenty-eighth National Convention of Aerospace Engineers held at Bangalore during November 14–15, 2014 organised by Karnataka State Centre, The Institution of Engineers (India).

References

1. J.S. Lilley, J.D. Hoffman, AIAA Paper No. 84-1416 (1984)
2. J.S. Lilley, J.D. Hoffman, JANNAF Propulsion Meeting (1985)
3. J.S. Lilley, AIAA Paper No. 85-1308 (1985)
4. J. Zhang, T.L. Jackson, J. Buckmaster, F. Najjar, J. Propuls. Power **27**(3), 642 (2011)
5. ICEM CFD-11, Installation and Overview, January—2007
6. ANSYS CFX, Release 11.0, Ansys Inc. Release Notes, January—2007
7. B.E. Launder, D.B. Spalding, Comp. Methods Appl. Mech. Eng. **3**, 269 (1974)
8. A. Javed, P.K. Sinha, D. Chakraborty, Def. Sci. J. **63**(6), 616 (2013)
9. S. Saha, P.K. Sinha, D. Chakraborty, in *Proceedings of 8th National Conference on Air breathing engines and Aerospace Propulsion*, 12–14 December 2006, at DIAT, Pune, pp 97–107
10. A. Javed, P. Manna, D. Chakraborty, Def. Sci. J. **62**(6), 369 (2012)
11. P. Manna, D. Chakraborty, Proc. Inst. Mech. Eng. Part G J. Aerosp. Eng. **219**(3), 205 (2005)
12. P. Manna, D. Chakraborty, J. Aerosp. Sci. Technol. **61**(2), 283 (2009)
13. S. Gordon, B.J. McBride, NASA RP-1311 Part I (1994)
14. S. Gordon, B.J. McBride, NASA RP-1311 Part II (1996)